Magnetic tunnel junctions with single-layer-graphene tunnel barriers

Wan Li,[1] Lin Xue,[1] H. D. Abruña,[2] and D. C. Ralph[1,3]
[1]*Physics Department, Cornell University, Ithaca, New York 14853, USA*
[2]*Department of Chemistry and Chemical Biology, Cornell University, Ithaca, New York 14853, USA*
[3]*Kavli Institute at Cornell, Cornell University, Ithaca, New York 14853, USA*
(Received 30 December 2013; revised manuscript received 14 February 2014; published 27 May 2014)

We report on the fabrication and characterization of magnetic tunnel junctions consisting of a single layer of graphene as the tunnel barrier, sandwiched between two metallic ferromagnetic electrodes. We employ a fabrication process chosen to minimize oxidation of the electrode materials at the ferromagnet/graphene interfaces. The devices have low resistance-area products of 1.5–6 $\Omega\,\mu m^2$, with low-temperature magnetoresistances of 1.5–3.4%. The temperature and bias dependencies of the resistance confirm that transport is dominated by tunneling processes rather than by any unintended pinholes.

DOI: 10.1103/PhysRevB.89.184418 PACS number(s): 85.75.Dd, 73.40.Gk, 72.80.Vp

Magnetic tunnel junctions (MTJs) are a central focus of spintronics research because of their usefulness in applications for magnetic random access memory [1,2], read heads for hard disk drives [3], and magnetic nano-oscillators for signal processing [4–6]. These applications generally require junctions with low resistance-area (*RA*) products, to minimize both the energy required for spin-transfer-torque manipulation and also the Johnson noise [7]. This motivates efforts to make the tunnel barrier in MTJs as thin as possible while still maintaining a large magnetoresistance. Previous research has investigated both traditional tunnel barrier materials such as Al_2O_3 (Refs. [8,9]) and MgO (Refs. [10,11]) and a wide variety of less common materials [12–15]. Here, we follow theoretical proposals [16–19] to explore the use of graphene [20,21] as a barrier material for MTJs, i.e., for a geometry in which electrons tunnel vertically through the graphene layer between two magnetic metal electrodes. Graphene is an attractive barrier material because layers with a thickness of just a single atom can be made pinhole-free over relatively large areas and are chemically inert. In addition, graphene is likely to present a low-energy tunnel barrier given that isolated single layers are zero-gap semiconductors. Theory [16–19] predicts that lattice-matched ferromagnet/(graphene or graphite)/ferromagnet devices may have large magnetoresistances, ranging from about 25% for a single-layer graphene barrier up to essentially perfect spin filtering for four layers and above. MTJs with graphene barriers have been made previously by several groups [22–24], but in all of these previous studies one of the magnetic electrodes was exposed to air (and in some cases immersed in water) in the course of depositing the graphene layer onto it, so that oxidation of this electrode likely affected the results [22]. These previous experiments measured resistance-area products for their junctions of $RA \sim 100{,}000\ \Omega\,\mu m^2$ (Ref. [22]), 35,000–75,000 $\Omega\,\mu m^2$ (Ref. [23]), and about 44 $\Omega\,\mu m^2$ (Ref. [24]) (but in this final case, the temperature dependence of the resistance was not consistent with tunneling). There have also been previous studies of ferromagnet/gold/graphene/ferromagnet [22] and ferromagnet/multilayer graphene/Al_2O_3/ferromagnet tunnel junctions [25].

We report the development of an alternative fabrication method designed to minimize oxidation of the magnetic electrodes, with which we achieved $RA = 1.5$–$6\ \Omega\,\mu m^2$, a reduction by more than 10^4 compared to Refs. [22] and [23], in junctions where the temperature and bias dependence confirmed that the transport mechanism was tunneling. The low-temperature magnetoresistance of our devices was 1.5–3.4%, which is smaller than the predictions in Refs. [16] and [17]. However, these predictions assumed lattice matching between the graphene and the magnetic electrodes, which is highly unlikely to be the case in our samples.

The scheme of our fabrication is to make a suspended graphene layer and then deposit ferromagnetic metal onto both sides to produce a MTJ in which the electrode/graphene interfaces are not exposed to air. Figure 1 illustrates the sample geometry and the steps of the fabrication process. The fabrication begins by making an array of circular holes (ranging from 250 nm to 3.2 μm in diameter) in a low-stress Si_3N_4 membrane on a 100 mm Si wafer. Photolithography and etching in an aqueous KOH solution are used to make suspended Si_3N_4 membranes approximately 100 μm across and 100 nm thick, each with one hole in the center. We coat these structures with 30–50 nm of Al_2O_3 grown by atomic layer deposition to preclude any unintended current leakage paths. We then grow graphene by chemical vapor deposition (CVD) on copper foil [26] and transfer the graphene to the hole array using poly(methyl methacrylate) (PMMA) as a supporting layer. The graphene/PMMA bilayer, after transfer, is suspended over the hole array with the PMMA side up. Our yield for making unbroken suspended graphene membranes is >90%. After thoroughly drying the devices at 170 °C for 30 min (this process also increases the adhesion of graphene to the substrate), we deposit one ferromagnetic electrode onto the bottom surface of the graphene, using 60 nm of permalloy (Py, $Ni_{81}Fe_{19}$) covered by 600 nm of Cu and 60 nm of Au. The PMMA layer is then removed by soaking the devices in a 1:1 mixture of acetone and dichloromethane solution, followed by an isopropyl alcohol rinse and a very gentle blow dry with nitrogen. As the last step of fabrication, we evaporate, through a shadow mask, a top magnetic electrode consisting of 60 nm of Co and 120 nm Au onto the exposed top graphene surface. The magnetic materials at the graphene interfaces of our devices are always protected by subsequently evaporated materials or the graphene itself, which, despite being a single-atomic-layer membrane, has been found to be a good barrier against oxidation [27,28]. The typical grain size in

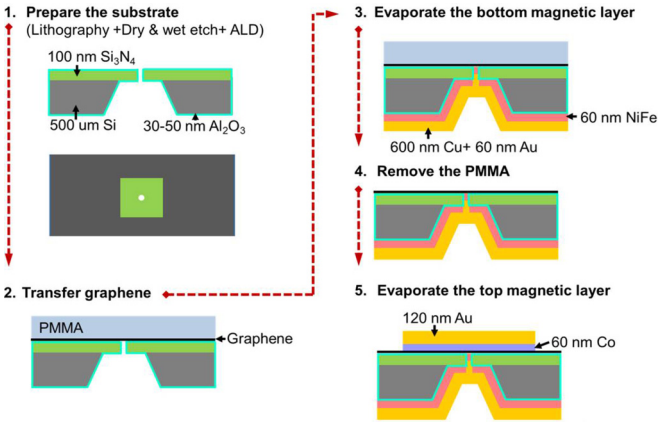

FIG. 1. (Color online) Procedure for fabricating the Py/Graphene/Co magnetic tunnel junctions using suspended graphene layers.

our CVD graphene layers as measured by diffraction-filtered electron microscopy [29] is 500 nm to 1 μm, so that our range of hole sizes spans the range from where grain boundaries should be rare to common. Details about the fabrication process are presented in the supplemental material [30]. We also attempted a fabrication procedure in which we removed the PMMA from the suspended graphene membranes first before any metal deposition, and then deposited the two magnetic electrodes on each side without breaking vacuum. However, we suffered a large percentage of broken membranes using this procedure.

Figure 2(a) shows a partially fabricated device after removing the PMMA layer (Fig. 1, Step 4). This optical image was taken from the top side of the device, and the junction corresponds to the central, bright yellow region. The bottom Py electrode is visible through the transparent graphene layer. A Raman spectrum [Fig. 2(b)] taken at the center

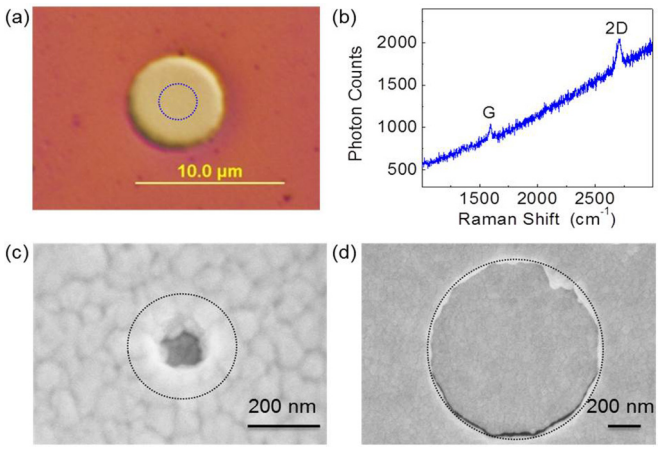

FIG. 2. (Color online) Characterization of the Py/Graphene/Co junctions during and after fabrication. (a) and (b) Optical image and Raman spectrum taken on top of the junction region before the top ferromagnetic electrode was evaporated. The dotted circle in (a) indicates the position where the Raman spectrum in (b) was taken. (c) and (d) SEM images of two different-sized junctions after the fabrication was completed. The added circles indicate the size of the hole in Si_3N_4 membrane before metal deposition.

TABLE I. Room-temperature resistances, room-temperature *RA* products, and magnetoresistances (*MR*) measured at low temperature (<10 K) and room temperature, for representative junctions.

Device Name	Diameter (μm)	Resistances (Ω)	*RA* product ($\Omega\,\mu$m^2)	Low-*T MR* (%)	Room-*T MR* (%)
A	0.25	55.8	2.7	1.8	0.7
B	0.25	71.2	3.5	3.2	1.7
C	0.25	64.5	3.2	3.4	0.9
D	0.25	440	21.6	1.5	0.9
E	0.25	30.6	1.5	N/A	0.9
F	0.25	126	6.2	N/A	1.3
G	0.34	37	3.4	N/A	0.3
H	0.74	10.8	4.6	N/A	0.7
I	1.36	54.5	79.1	N/A	0.5
J	1.74	28.8	68.4	0.8	0.3

of the junction region [dotted circle in Fig. 2(a)] contained pronounced 2D (2700 cm^{-1}) and G (1590 cm^{-1}) peaks, with the 2D peak amplitude more than twice that of the G peak, confirming the existence of monolayer graphene over the junction region. No D peak is observed above the noise level, indicating a reasonably high quality of graphene. Scanning electron microscope (SEM) images of the junctions, after all the fabrication processes were completed, are shown in Figs. 2(c) and 2(d) for different-sized junctions.

The device diameter, resistance, *RA* product, and magnetoresistance of 10 representative junctions are presented in Table I. Most junctions yielded an *RA* product of 1.5–6 $\Omega\,\mu$m^2. Below, we discuss evidence that indicates the transport in these devices occurs by tunneling and not via metallic shorts through pinholes in the graphene. A few junctions had higher *RA* products, in the range 20–80 $\Omega\,\mu$m^2. These higher values appear to have some correlation with the larger device diameters. They might be due to oxidation of the lower magnetic electrode through imperfections in the graphene (which might be more common in larger devices) or residual PMMA remaining on the graphene despite our cleaning procedure.

To ensure that the signals measured in our test devices (Table I) came from the graphene junction area alone, we also fabricated control devices in parallel with the test devices on the same substrates. The control devices had the same structure as the test devices, except that no hole was etched into the Si_3N_4 membrane, and thus no MTJs could be formed. The resistance of the control devices was $\sim$30 MΩ at room temperature (supplemental material, Fig. S4 [30]) and much greater at low temperature, or $\sim 10^5$ higher at room temperature than that of the graphene junctions (typically 10–100 Ω). Therefore, electrical currents hopping or tunneling through the Si_3N_4 membrane should not contribute significantly to measurements of the graphene MTJ devices.

We determined that the mechanism of transport through the graphene consisted of tunneling, as opposed to metallic transport via pinholes, by studying the bias and temperature dependencies of the resistance. Figure 3(a) shows the differential resistance in the parallel magnetic state (R_p) of a representative Py/Graphene/Co junction at different dc bias voltages, measured in a magnetic field of 1500 Oe in the sample

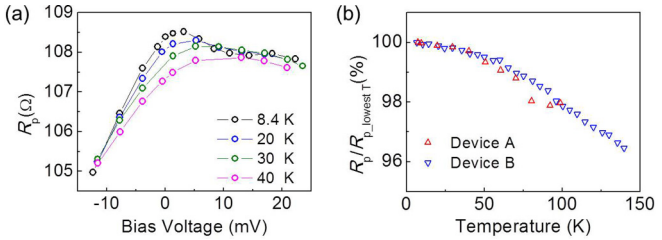

FIG. 3. (Color online) Bias and temperature dependencies of junction resistance. (a) The bias dependence of a junction (device B) measured at four different temperatures. (b) The temperature dependence of resistance for devices A and B. The junctions were magnetized in a parallel alignment with a magnetic field of 1500 Oe.

plane. The differential resistance has a maximum at a bias voltage close to zero and decreases with increasing bias magnitude, consistent with tunneling transport. The bias dependence exhibits a clear asymmetry, with the differential resistance decreasing faster in the negative bias direction (corresponding to electron flow from the Py to the Co) for all devices studied. This asymmetry is likely caused by the different work functions of the two different ferromagnetic materials used as electrodes. We estimated the barrier parameters by fitting the bias dependence at 40 K to the Brinkman model for transport in an asymmetric tunnel junction [31] (supplemental material [30]). The fit (supplemental material, Fig. S5 [30]) yielded an effective barrier thickness of 12.1 ± 0.1 Å, a barrier height of 90 ± 3 meV, and a work function difference between the electrodes of 59 ± 3 meV; the latter is consistent with known work function values [32]. Although graphene is a zero-gap semiconductor in its free-standing state, theoretical studies suggest that interactions between graphene and neighboring electrode atoms may open a gap in graphene [16,17]. This could explain the nonzero but still relatively low barrier height suggested by the fitting. Figure 3(b) shows the temperature dependence of the resistance of devices A and B, normalized in the form $R_p(T)/R_p$ (low_temperature). The resistances of the devices decrease moderately as the temperature increases, again consistent with tunneling transport through a weak barrier [33].

Resistances as a function of swept magnetic field are shown in Fig. 4 for (a) a device with a relatively large diameter (1.74 μm) and a large RA value (68 $\Omega\,\mu m^2$) and (b) one with a smaller diameter (250 nm) and a low RA value (2.7 $\Omega\,\mu m^2$). A saturated low-resistance state (R_p) was observed for magnetic field magnitudes large enough to align the magnetizations of the electrodes, with an increased resistance upon sweeping through zero field due to electrode misalignment. The measured magnetoresistance (MR) values, defined by $MR = (R_{max} - R_p)/R_p$, where R_{max} is the maximum resistance in the resistance vs field curve, are listed for room temperature and low temperature in the last two columns of Table I. We observe MRs of 1.5–3.4% below 10 K, comparable to the 2% MR reported previously for the much higher resistance junctions of Cobas *et al.* [23]. The value is, however, significantly lower than the theoretical prediction (~25% for single-layer graphene), perhaps due to the lack of lattice matching for our graphene/ferromagnet interfaces [16,17].

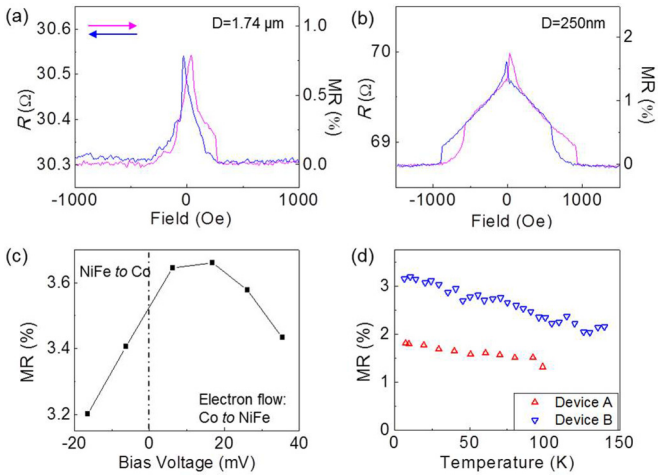

FIG. 4. (Color online) Magnetoresistance characteristics of Py/Graphene/Co MTJs. (a) and (b) Resistance and magnetoresistance vs applied magnetic field for two representative junctions, (a) a large junction: diameter = 1.74 μm (device J) and (b) a small junction: diameter = 250 nm (device A). (c) Bias dependence of the magnetoresistance of device C (250 nm) at 6.1 K. (d) Temperature dependence of the magnetoresistance for devices A and B.

For the larger junctions with larger RA values [Fig. 4(a)], the transitions between the high- and low-resistance states are observed at relatively low magnetic field strengths (~30 Oe). These values are comparable to the coercive fields of the ferromagnetic films used (15–20 Oe for Co and 1–10 Oe for Py), indicative of conventional reversal of magnetization orientations via domain wall motion without any obvious interaction between the electrodes. However, for the junctions with smaller diameters and smaller RA values [Fig. 4(b)], the magnetoresistance curves have broad gradual slopes extending to almost 1000 Oe, with a region of hysteresis between about 600 Oe and 1000 Oe bounded by abrupt switching events. This unusual resistance vs field behavior was consistently observed for all junctions <1 μm in diameter with RA values in the range 1.5–6 $\Omega\,\mu m^2$, and it suggests that magnetic reorientation in these samples occurs through a combination of gradual rotation followed by discontinuous jumps. We suggest that these features are due to strong antiferromagnetic coupling across the graphene in the devices with smaller RA values. When this coupling is stronger than the magnetic anisotropy, the effect of an applied magnetic field will be to tilt the moments away from antiparallel alignment while rotating them so that the resulting net moment is along the field direction, in analogy to the spin-flop transition in an antiferromagnet. In Fig. 4(b), the electrodes resist full saturation to the parallel state for a field less than about 1000 Oe, indicating a very substantial antiferromagnetic coupling, i.e., much stronger than the coercive fields of the bulk films (a few tens of Oe). Recent theoretical studies have also suggested the existence of graphene-mediated antiferromagnetic exchange coupling between two magnetic electrodes [34,35]. If the large RA values in our larger samples are due to unintended oxidation from air penetrating through defects in the graphene, as discussed above, this could explain the absence of very strong exchange coupling in those devices.

The bias and temperature dependencies of magnetoresistance are shown in Figs. 4(c) and 4(d). The magnetoresistance depends strongly on the bias voltage, with a peak near zero bias and diminution at higher bias magnitudes [Fig. 4(c)]. Such behavior is typical of tunneling magnetoresistance with a wide variety of tunnel barriers [36,37]. The bias voltage dependence of the magnetoresistance exhibits some asymmetry, decreasing faster at negative biases. Like the asymmetry in the bias dependence of the differential resistance (see above), this likely reflects the different work functions and densities of states for the two different ferromagnetic electrodes. Figure 4(d) shows the temperature dependence of the magnetoresistance for devices A and B. Higher magnetoresistance is observed at lower temperatures. This behavior is also typical of MTJs and can be attributed to the excitation of spin waves in the ferromagnetic material, which decrease the effective tunneling polarization [1,38].

One issue worthy of further investigation is the breakdown voltage of the graphene junctions. We did not fabricate enough devices to study this in detail, but we did observe breakdown in one device at a bias voltage of just 30 mV. (We limited our measurements of other devices to low biases for this reason.) Breakdown led to a shorted device ($<10\ \Omega$) in which the bias dependence of the resistance was no longer consistent with tunneling. (See Fig. S6 and the corresponding discussion in the supplemental material [30].) We have not determined if breakdown at low voltage might be an intrinsic property of single-layer graphene junctions, or whether it might be associated with grain boundaries or other defects in the graphene.

In summary, we have reported a fabrication procedure for making magnetic tunnel junctions using single-layer graphene as the tunnel barrier, in a way that minimizes oxidation of the magnetic electrodes. The junction resistances exhibit temperature and bias dependencies consistent with tunneling transport, with typical RA products of 1.5–6 $\Omega\,\mu\mathrm{m}^2$, which is a factor of 10^4 times smaller than previous experiments in which magnetic electrodes were exposed to air [22,23]. The magnetoresistance of our devices is 1.5–3.4% at temperatures below 10 K.

We thank Sufei Shi, Eugenia Tam, Cen Tan, Zenghui Wang, and Ke Xu for discussion and advice. This work was supported by the Cornell Center for Materials Research with funding from the National Science Foundation (NSF) MRSEC program (Grant No. DMR-1120296) and by the NSF (Grant No. DMR-1010768). We also acknowledge support from the NSF to the Cornell Nanofabrication Facility/NNIN.

[1] J. A. Katine and E. E. Fullerton, J. Magn. Magn. Mater. **320**, 1217 (2008).
[2] N. D. Rizzo, D. Houssameddine, J. Janesky, R. Whig, F. B. Mancoff, M. L. Schneider, M. DeHerrera, J. J. Sun, K. Nagel, S. Deshpande, H.-J. Chia, S. M. Alam, T. Andre, S. Aggarwal, and J. M. Slaughter, IEEE Trans. Magn. **49**, 4441 (2013).
[3] Z. Jia and R. D. K. Misra, Mater. Techn. **26**, 191 (2011).
[4] A. Deac, A. Fukushima, H. Kubota, H. Maehara, Y. Suzuki, S. Yuasa, Y. Nagamine, K. Tsunekawa, D. D. Djayaprawira, and N. Watanabe, Nature Phys. **4**, 803 (2008).
[5] D. Houssamedine, S. H. Florez, J. A. Katine, J.-P. Michel, U. Ebels, D. Mauri, O. Ozatay, B. Delaet, B. Viala, L. Folks, B. D. Terris, and M.-C. Cyrille, Appl. Phys. Lett. **93**, 022505 (2008).
[6] A. Dussaux, B. Georges, J. Grollier, V. Cros, A. V. Khvalkovskiy, A. Fukushima, M. Konoto, H. Kubota, K. Yakushiji, S. Yuasa, K. A. Zvezdin, K. Ando, and A. Fert, Nat. Commun. **1**, 8 (2010).
[7] S. Yuasa and D. D. Djayaprawira, J. Phys. D. Appl. Phys. **40**, R337 (2007).
[8] J. S. Moodera, L. R. Kinder, T. M. Wong, and R. Meservey, Phys. Rev. Lett. **74**, 3273 (1995).
[9] T. Miyazaki and N. Tezuka, J. Magn. Magn. Mater. **139**, L231 (1995).
[10] S. S. P. Parkin, C. Kaiser, A. Panchula, P. M. Rice, B. Hughes, M. Samant, and S.-H. Yang, Nature Mater. **3**, 862 (2004).
[11] S. Yuasa, T. Nagahama, A. Fukushima, Y. Suzuki, and K. Ando, Nature Mater. **3**, 868 (2004).
[12] Zheng Gao, Sining Mao, Khoung Tran, Janusz Nowak, and Jian Chen, US Patent No. 6,791,806 B1, September 14, 2004.
[13] J. Z. Sun, W. J. Gallagher, P. R. Duncombe, L. Krusin-Elbaum, R. A. Altman, A. Gupta, Y. Lu, G. Q. Gong, and G. Xiao, Appl. Phys. Lett. **69**, 3266 (1996).
[14] C. Kaiser, S. Van Dijken, S.-H. Yang, H. Yang, and S. S. P. Parkin, Phys. Rev. Lett. **94**, 247203 (2005).
[15] V. Garcia, M. Bibes, J.-L. Maurice, E. Jacquet, K. Bouzehouane, J.-P. Contour, and A. Barthelemy, Appl. Phys. Lett. **87**, 212501 (2005).
[16] V. M. Karpan, P. A. Khomyakov, A. A. Starikov, G. Giovannetti, M. Zwierzycki, M. Talanana, G. Brocks, J. van den Brink, and P. J. Kelly, Phys. Rev. B **78**, 195419 (2008).
[17] V. M. Karpan, G. Giovannetti, P. A. Khomyakov, M. Talanana, A. A. Starikov, M. Zwierzycki, J. van den Brink, G. Brocks, and P. J. Kelly, Phys. Rev. Lett. **99**, 176602 (2007).
[18] O. V. Yazyev and A. Pasquarello, Phys. Rev. B **80**, 035408 (2009).
[19] K. K. Saha, A. Blom, K. S. Thygesen, and B. K. Nikolic, Phys. Rev. B **85**, 184426 (2012).
[20] K. S. Novoselov, A. K. Geim, S. V. Morozov, D. Jiang, Y. Zhang, S. V. Dubonos, I. V. Grigorieva, and A. A. Firsov, Science **306**, 666 (2004).
[21] K. S. Novoselov, V. I. Falko, L. Colombo, P. R. Gellert, M. G. Schwab, and K. Kim, Nature **490**, 192 (2012).
[22] T. M. G. Mohiuddin, E. Hill, D. Elias, A. Zhukov, K. Novoselov, and A. Geim, IEEE Trans. Magn. **44**, 2624 (2008).
[23] E. Cobas, A. L. Friedman, O. M. J. van't Erve, J. T. Robinson, and B. T. Jonker, Nano Lett. **12**, 3000 (2012).
[24] M. Z. Iqbal, M. W. Iqbal, J. H. Lee, Y. S. Kim, S.-H. Chun, and J. Eom, Nano Res. **6**, 373 (2013).
[25] B. Dlubak, M.-B. Martin, R. S. Weatherup, H. Yang, C. Deranlot, R. Blume, R. Schloegl, A. Fert, A. Anane, S. Hofmann, P. Seneor, and J. Robertson, ACS Nano **6**, 10930 (2012).
[26] X. Li, W. Cai, J. An, S. Kim, J. Nah, D. Yang, R. Piner, A. Velamakanni, I. Jung, E. Tutuc, S. K. Banerjee, L. Colombo, and R. S. Ruoff, Science **324**, 1312 (2009).

[27] S. Chen, L. Brown, M. Levendorf, W. Cai, S.-Y. Ju, J. Edgeworth, X. Li, C. W. Magnuson, A. Velamakanni, R. D. Piner, J. Kang, J. Park, and R. S. Ruoff, ACS Nano **5**, 1321 (2011).

[28] J. Coraux, A. T. N'Diaye, N. Rougemaille, C. Vo-Van, A. Kimouche, H.-X. Yang, M. Chshiev, N. Bendiab, O. Fruchart, and A. K. Schmid, J. Phys. Chem. Lett. **3**, 2059 (2012).

[29] P. Y. Huang, C. S. Ruiz-Vargas, A. M. van der Zande, W. S. Whitney, M. P. Levendorf, J. W. Kevek, S. Garg, J. S. Alden, C. J. Hustedt, Y. Zhu, J. Park, P. L. McEuen, and D. A. Muller, Nature **469**, 389 (2011).

[30] See Supplemental Material at http://link.aps.org/supplemental/10.1103/PhysRevB.89.184418 for detailed information about materials growth and device fabrication, measurement procedures, control experiments, data analysis, and measurements on a device that underwent tunnel barrier breakdown.

[31] W. F. Brinkman, R. C. Dynes, and J. M. Rowell, J. Appl. Phys. **41**, 1915 (1970).

[32] W. M. Haynes, *CRC Handbook of Chemistry and Physics*, 94th edition (CRC Press Boca Raton, FL, 2013-2014), pp. 12–124.

[33] B. J. Jönsson-Åkerman, R. Escudero, C. Leighton, S. Kim, I. K. Schuller, and D. A. Rabson, Appl. Phys. Lett. **77**, 1870 (2000).

[34] B. Li, L. Chen, and X. Pan, Appl. Phys. Lett. **98**, 133111 (2011).

[35] D. Kim, A. Hashmi, C. Hwang, and J. Hong, Appl. Phys. Lett. **102**, 112403 (2013).

[36] S. Zhang, P. M. Levy, A. C. Marley, and S. S. P. Parkin, Phys. Rev. Lett. **79**, 3744 (1997).

[37] S. O. Valenzuela, D. J. Monsma, C. M. Marcus, V. Narayanamurti, and M. Tinkham, Phys. Rev. Lett. **94**, 196601 (2005).

[38] C. H. Shang, J. Nowak, R. Jansen, and J. S. Moodera, Phys. Rev. B **58**, R2917 (1998).